Nonaffine Helicopter Control Design and Implementation Based on a Robust Explicit Nonlinear Model Predictive Control

Joohwan Seo, Seongwon Lee, Joonho Lee, and Jongeun Choi, *Member, IEEE*

***Abstract*— Control design for a helicopter is a challenging problem because of its nonaffine inputs, its underactuated characteristics, and highly coupled dynamics. To solve a control problem of the helicopter under model uncertainties and disturbance present environments, an explicit nonlinear model predictive control (ENMPC), a dynamic inversion (DI), and an extended high-gain observer (EHGO) are combined in a multi-time-scale fashion. The multi-time-scale scaled structure and the ENMPC provide the framework of the control design, the DI deals with nonaffine control inputs, and the EHGO estimates the unmeasured system states and uncertainties. The proposed control design is discretized to be implemented on a small-scale helicopter. The successful outdoor experiments with the proposed control implemented on autopilot hardware demonstrate the validity of our approach in the presence of model uncertainties and wind disturbances.**

***Index Terms*— Dynamic inversion (DI), explicit nonlinear model predictive control (ENMPC), extended high-gain observer (EHGO), nonaffine control inputs, underactuated mechanical systems.**

I. Introduction

With the advance of computation power of embedded computers, battery capacities, and motor performances, unmanned aerial vehicle (UAV) industries are growing and applied rapidly in everyday life. Especially, helicopters have their superiority over quadrotors on agile movement and the faster response despite its unstable dynamics [1]–[3]. The control design for high-performance autonomous helicopters is challenging. This is because helicopters are underactuated mechanical and highly nonlinear systems. In addition, the exogenous disturbances and model uncertainties make the control design of a helicopter more difficult [4], [5].

A popular approach to deal with the underactuated mechanical system is a time-scale separation [6]. The time-scale separation lies on the concept that the inner loop is faster than the outer loop so that the controllers are designed to overcome the lack of the number of inputs [7], [8].

Sliding-mode and backstepping techniques for helicopter control are widely employed to deal with the underactuated mechanical systems since the helicopter model can be approximated by a strict-feedback form. Based on the backstepping technique, other approaches are combined to deal with disturbances and uncertainties [6], [9], [10]. In [9], the passivity-based adaptive backstepping control for quadrotors, i.e., underactuated mechanical systems, was proposed. The backstepping control is utilized to deal with underactuated mechanical systems, whereas parameter uncertainties are dealt with using adaptive law. In [10], continuous sliding mode control with disturbance observer (DOB-CSMC) was utilized for the helicopter control. The continuous-sliding-mode control was utilized to reduce chattering, while the disturbance observer was employed to deal with both matched and mismatched uncertainties. Some approach utilizes receding horizon estimator to deal with time-varying aerodynamic parameters in [11].

Uncertainty estimators based on neural networks have been adopted by many researchers in the control design of UAVs. In [12], the neural networks are utilized to estimate uncertainties and disturbances for the robust control of the helicopter. The neural networks are trained to learn the quadrotor dynamics when landing in [13], with feedback linearization. However, the neural networks are not readily applicable to vehicle onboard since the neural networks often require heavy computations.

Helicopter control designs using feedback linearization with disturbance observers were proposed in [4] and [14]. An active disturbance rejection control was suggested in [4], using the dynamic feedback linearization [15]. In [14], explicit nonlinear model predictive control (ENMPC) provided optimal control inputs for the tracking control with a disturbance observer. However, the aforementioned methods considered approximated dynamics, i.e., linearized control inputs, which results in a smaller region of attraction than nonaffine control inputs.

In order to deal with nonaffine control inputs, a dynamic inversion (DI) scheme was employed in [16], based on the time-scale separation. In addition, the extended high-gain observer (EHGO) was used to estimate the model uncertainties and external disturbances for rotational dynamics. In [17], the output feedback control design in the presence of uncertainties was presented. The output feedback control with DI was designed for a quadrotor helicopter in [18], and its implementation was presented in [19].

In this brief, we propose a control design for the tracking problem of a small-scale helicopter. The proposed control

Manuscript received October 7, 2020; revised January 2, 2021; accepted February 28, 2021. Date of publication April 6, 2021; date of current version February 10, 2022. Manuscript received in final form March 24, 2021. This work was supported in part by the National Research Foundation of Korea Grant funded by the Korean Government (Ministry of Science and Information Technology) under Grant 2021R1A2B5B01002620 and in part by the Ministry of Culture, Sports and Tourism (MCST) and the Korea Creative Content Agency (KOCCA) through the Culture Technology (CT) Research and Development Program 2019 under Grant R2019020038. Recommended by Associate Editor L. Fagiano. *(Corresponding author: Jongeun Choi.)*

Joohwan Seo, Seongwon Lee, and Jongeun Choi are with the School of Mechanical Engineering, Yonsei University, Seoul 03722, Republic of Korea (e-mail: larban@yonsei.ac.kr; rmdwjdrhkrkatk@yonsei.ac.kr; jongeunchoi@yonsei.ac.kr).

Joonho Lee is with the Electrical and Controls Systems Research Lab, General Motors Research and Development, Warren, MI 48092 USA (e-mail: ljah1s@gmail.com).

This article has supplementary material provided by the authors and color versions of one or more figures available at https://doi.org/10.1109/TCST.2021.3069106.

Digital Object Identifier 10.1109/TCST.2021.3069106

method is used to overcome the uncertainties and underactuated mechanics of a helicopter and to guarantee optimal tracking. A multi-time-scale structure is employed to deal with the underactuated mechanical system. Based on the multi-time-scale structure, the ENMPC provides a framework of the control design for optimal trajectory tracking. The DI is added to deal with nonaffine control inputs. The EHGO is utilized to estimate the model uncertainties, unmeasured system states, and external disturbances. The main contributions are listed as follows.

1) A novel control design for a small-scale helicopter is developed in this brief. This novel control design utilizes the DI to the ENMPC framework to increase the region of attraction by dealing with nonaffine control inputs, deal with input uncertainties, and guarantee optimal tracking.
2) The stability of its continuous-time closed-loop system is analyzed.
3) The proposed control design is discretized for the implementation of the small-scale helicopter. Benchmark simulation results of the trajectory tracking are presented to show the effectiveness and outperformance of the proposed control design.
4) To demonstrate the feasibility of our control design, we show the experimental results in the outdoor, where the incessant disturbances are present, on the small-scale helicopter using the embedded board.

This brief is an extended version of the conference papers [20] and [17]. In contrast to [20], in this brief, the mathematical stability analysis in continuous time is conducted, the benchmark simulation results to show the outperformance of our control design are presented, and the outdoor experiment is performed to validate the proposed control design. Compared to [17], the optimality conditions from the ENMPC have been employed to enhance the control performance.

This brief is organized as follows. In Section II, a helicopter model and corresponding state-space equations are presented. In Section III, we design the helicopter controller in continuous time, and the stability analysis is provided. In Section IV, the discretization of the proposed control design, a hardware setup, and experimental results are shown. Finally, concluding remarks are discussed in Section V. The standard notation will be used in this brief.

II. Helicopter Dynamics

The coordinate system used throughout this brief is shown in Fig. 1—north-east-down (NED) coordinates. Following the generalized control design process, we utilize the helicopter model in [17], which has rotational and translational dynamics. The helicopter model for the rotational dynamics is

$$\dot{\Theta} = A\Theta + BF_R + B\sigma_\Theta, \quad Y_\Theta = C\Theta \tag{1}$$

where $\Theta = [\phi_1, \phi_2, \theta_1, \theta_2, \psi_1, \psi_2]^{\mathrm{T}} = [\phi, \dot{\phi}, \theta, \dot{\theta}, \psi, \dot{\psi}]^{\mathrm{T}} \in \mathbb{R}^6$, where the angles ϕ, θ, and ψ are along x^b, y^b, and z^b, respectively, and $F_R = [f_\phi, f_\theta, f_\psi]^{\mathrm{T}} = F_R(\Theta, u_r, u_t)$. The uncertainty is $\sigma_\Theta = [\sigma_\phi, \sigma_\theta, \sigma_\psi]^{\mathrm{T}} \in \mathbb{R}^3$ in the form of angular acceleration. In this brief, we deal with the domain D_Θ given by

$$\begin{aligned} D_\Theta &= D_\phi \times D_\theta \times D_\psi \\ D_\phi &= \{-a_\phi \le \phi_1 \le a_\phi\} \times \{-b_\phi \le \phi_2 \le b_\phi\} \\ D_\theta &= \{-a_\theta \le \theta_1 \le a_\theta\} \times \{-b_\theta \le \theta_2 \le b_\theta\} \\ D_\psi &= \{-a_\psi \le \psi_1 \le a_\psi\} \times \{-b_\psi \le \psi_2 \le b_\psi\} \end{aligned}$$

where $0 < a_i < \pi/2$ and $b_i > 0$ are bounded for $i \in \{\phi, \theta, \psi\}$. The matrices A and B are $A =$ block diag$[A_1, A_1, A_1]$ and $B =$ block diag$[B_1, B_1, B_1]$. The measurement Y_Θ is from inertial measurement units (IMU) and $C =$ block diag$[C_1, C_1, C_1]$. A_1, B_1, and C_1 are matrices with

$$A_1 = \begin{bmatrix} 0 & 1 \\ 0 & 0 \end{bmatrix}, \quad B_1 = \begin{bmatrix} 0 \\ 1 \end{bmatrix}, \quad C_1 = \begin{bmatrix} 1 & 0 \end{bmatrix}. \tag{2}$$

One may find the equations for $F_R(\Theta, u_r, u_t) = [f_\phi, f_\theta, f_\psi]^{\mathrm{T}}$ in Section S1 of the Supplementary Material or in [20].

In addition, $u_r = [T_t, a_{1s}, b_{1s}]^{\mathrm{T}}$ is the rotational control input, and $u_t = [T_m, \phi_d, \theta_d]^{\mathrm{T}}$ is the translational control input, where T_t is the thrust force of tail rotor; a_{1s} is main rotor tip's angle with respect to the x-axis; b_{1s} is main rotor tip's angle with respect to the y-axis; T_m is main rotor's thrust force; ϕ_d is the reference of ϕ; and θ_d is the reference of θ. Note that control inputs of translational dynamics ϕ_d and θ_d act as references to rotational dynamics. The inputs u_t and u_r are defined in $u_t \in D_t \subset \mathbb{R}^3$ and $u_r \in D_r \subset \mathbb{R}^3$, and the sets D_t and D_r are compact.

The helicopter model for the translational dynamics can be approximated as suggested in [8] and [21], as follows:

$$\dot{\chi} = A\chi + BF_T + B\sigma_\chi, \quad Y_\chi = C\chi \tag{3}$$

where $\chi = [x_1, x_2, y_1, y_2, z_1, z_2]^{\mathrm{T}} = [x, \dot{x}, y, \dot{y}, z, \dot{z}]^{\mathrm{T}} \in D_\chi$, where $D_\chi \in \mathbb{R}^6$ is bounded, and x, y, z are from the global coordinate system. The uncertainty is $\sigma_\chi = [\sigma_x, \sigma_y, \sigma_z]^{\mathrm{T}} \in \mathbb{R}^3$ in the form of the acceleration, and $F_T = [f_x, f_y, f_z]^{\mathrm{T}} = F_T(\Theta, u_t) \in \mathbb{R}^3$. One may also find the equations of $F_T(\Theta, u_t)$ in the Supplementary Material or in [20].

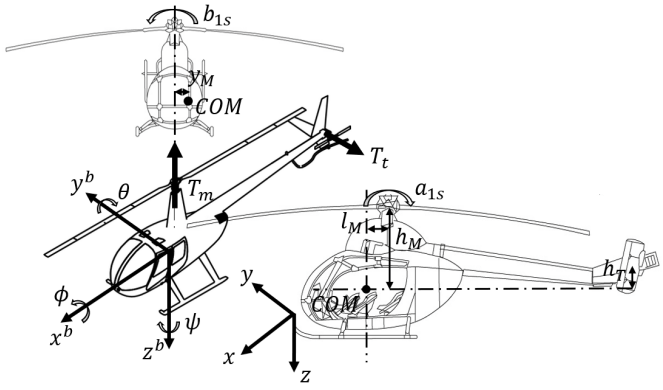

Fig. 1. Model diagram of the helicopter.

III. Control Design in Continuous Time

A. Applying Dynamic Inversion to ENMPC Framework

Based on the framework of the ENMPC, the DI scheme is applied, and the EHGO is employed to deal with exogenous

disturbances. Furthermore, we employ time-scale structure to cope with an underactuated characteristic of the helicopter.

First, using the method suggested in [22], we obtain the cost function for the rotational dynamics J_Θ and the cost function for the translational dynamics J_χ. The necessary condition for the optimality of the rotational dynamics is given by [22]

$$\frac{\partial J_\Theta}{\partial u_r} = 0. \tag{4}$$

Equation (4) leads to the following equation:

$$\begin{aligned}\frac{\partial J_\Theta}{\partial u_r} &= \left[\frac{\partial J_\Theta}{\partial T_t}, \frac{\partial J_\Theta}{\partial a_{1s}}, \frac{\partial J_\Theta}{\partial b_{1s}}\right]^{\mathrm{T}} \\ &= \left(\frac{\partial F_R}{\partial u_r}\right)^{\mathrm{T}} \\ &\quad \times \begin{bmatrix} k_1(\phi_1 - \phi_r) + k_2\left(\phi_2 - \dot{\phi}_r\right) + \left(f_\phi - \ddot{\phi}_r\right) + \sigma_\phi \\ k_1(\theta_1 - \theta_r) + k_2\left(\theta_2 - \dot{\theta}_r\right) + \left(f_\theta - \ddot{\theta}_r\right) + \sigma_\theta \\ k_1(\psi_1 - \psi_r) + k_2\left(\psi_2 - \dot{\psi}_r\right) + \left(f_\psi - \ddot{\psi}_r\right) + \sigma_\psi \end{bmatrix} \\ &= 0 \end{aligned} \tag{5}$$

where gains k_1 and k_2 are given with the rotational time horizon ϵ_r as

$$k_1 = \frac{10}{3\epsilon_r^2}, \quad k_2 = \frac{5}{2\epsilon_r}. \tag{6}$$

The detailed derivation can be found in the appendix of [20] and omitted in this brief. In order to utilize the nonaffine control inputs, we applied a control scheme proposed in [23]–[25]—the approximate DI. The control input u_r that achieves (5) in our multi-time-scale structure is derived using the DI as follows:

$$\begin{aligned}\epsilon_3 \dot{u}_r &= -\left(\frac{\partial F_R}{\partial u_r}\right)^{\mathrm{T}} \\ &\quad \times \begin{bmatrix} k_1(\phi_1 - \phi_r) + k_2\left(\phi_2 - \dot{\phi}_r\right) + \left(f_\phi - \ddot{\phi}_r\right) \\ k_1(\theta_1 - \theta_r) + k_2\left(\theta_2 - \dot{\theta}_r\right) + \left(f_\theta - \ddot{\theta}_r\right) \\ k_1(\psi_1 - \psi_r) + k_2\left(\psi_2 - \dot{\psi}_r\right) + \left(f_\psi - \ddot{\psi}_r\right) \end{bmatrix} \end{aligned} \tag{7}$$

for $\epsilon_3 \ll 1$. We also note that the uncertainty σ_Θ is assumed to be 0 in the state feedback, not appearing in (7).

Since the rotational references ϕ_r and θ_r are control inputs of the slower translational dynamics, we may consider $\phi_r \approx \phi_d$ and $\theta_r \approx \theta_d$ as constant, i.e., $\dot{\phi}_r, \ddot{\phi}_r, \dot{\theta}_r, \ddot{\theta}_r$ are all 0—see [17]. Therefore, (7) can be further approximated by

$$\begin{aligned}\epsilon_3 \dot{u}_r &= -\left(\frac{\partial F_R}{\partial u_r}\right)^{\mathrm{T}} \begin{bmatrix} k_1(\phi_1 - \phi_d) + k_2\phi_2 + f_\phi \\ k_1(\theta_1 - \theta_d) + k_2\theta_2 + f_\theta \\ k_1(\psi_1 - \psi_r) + k_2\psi_2 + f_\psi \end{bmatrix} \\ &= -\left(\frac{\partial F_R}{\partial u_r}\right)^{\mathrm{T}} F_\Theta(\Theta, u_t, u_r, \psi_r) \end{aligned} \tag{8}$$

where

$$\begin{aligned} F_\Theta &= F_R(\Theta, u_r, u_t) - F_{R,r}(\Theta, u_t, \psi_r) \\ F_{R,r}(\Theta, u_t, \psi_r) &= \begin{bmatrix} -k_1(\phi_1 - \phi_d) - k_2\phi_2 \\ -k_1(\theta_1 - \theta_d) - k_2\theta_2 \\ -k_1(\psi_1 - \psi_r) - k_2\psi_2 \end{bmatrix} \end{aligned}$$

which is the same form of the controller with the DI in [17]. Note that the gains (6) are the ones to achieve the optimal desired closed-loop dynamics F_Θ. The rotational DI controller is based on the following assumptions.

Assumption 1:
1) In the domains D_χ and D_Θ, the Jacobian matrix $(\partial F_R/\partial u_r)$ is nonsingular.
2) There is a solution u_r^* such that $F_\Theta(\Theta, u_r^*, u_t, \psi_r) = 0$ from (8).
3) $F_\Theta(\Theta, u_r, u_t, \psi_r)$ is Lipschitz in its arguments on the domains D_χ, D_Θ, D_r, and D_t.

In the same manner, solving the necessary condition for the optimality of translational dynamics, the following equation is derived:

$$\begin{aligned}\frac{\partial J_\chi}{\partial u_t} &= \left[\frac{\partial J_\chi}{\partial T_m}, \frac{\partial J_\chi}{\partial \phi_d}, \frac{\partial J_\chi}{\partial \theta_d}\right]^{\mathrm{T}} \\ &= \left(\frac{\partial F_T}{\partial u_t}\right)^{\mathrm{T}} \\ &\quad \times \begin{bmatrix} k_p(x_1 - x_r) + k_v(x_2 - \dot{x}_r) + (f_x - \ddot{x}_r) + \sigma_x \\ k_p(y_1 - y_r) + k_v(y_2 - \dot{y}_r) + \left(f_y - \ddot{y}_r\right) + \sigma_y \\ k_p(z_1 - z_r) + k_v(z_2 - \dot{z}_r) + (f_z - \ddot{z}_r) + \sigma_z \end{bmatrix} \\ &= 0 \end{aligned} \tag{9}$$

where gains k_p and k_v are given using the translational time horizon ϵ_t as

$$k_p = \frac{10}{3\epsilon_t^2}, \quad k_v = \frac{5}{2\epsilon_t}. \tag{10}$$

Considering that the translational dynamics are slower than the rotational dynamics, the translational time horizon ϵ_t is larger enough than the rotational time horizon ϵ_r.

The control input u_t of (9) is derived in the same manner as the rotational controller (7) is

$$\begin{aligned}\epsilon_2 \dot{u}_t &= -\left(\frac{\partial F_T}{\partial u_t}\right)^{\mathrm{T}} \begin{bmatrix} k_p(x_1 - x_r) + k_v(x_2 - \dot{x}_r) + (f_x - \ddot{x}_r) \\ k_p(y_1 - y_r) + k_v(y_2 - \dot{y}_r) + \left(f_y - \ddot{y}_r\right) \\ k_p(z_1 - z_r) + k_v(z_2 - \dot{z}_r) + (f_z - \ddot{z}_r) \end{bmatrix} \\ &= -\left(\frac{\partial F_T}{\partial u_t}\right)^{\mathrm{T}} F_\chi(\chi, \Theta, u_t, \chi_r) \end{aligned} \tag{11}$$

where $\epsilon_2 \ll 1$, and

$$\begin{aligned} F_\chi &= F_T(\Theta, u_t) - F_{T,r}(\chi, \chi_r) \\ F_{T,r}(\chi, \chi_r) &= \begin{bmatrix} -k_p(x_1 - x_r) - k_v(x_2 - \dot{x}_r) + \ddot{x}_r \\ -k_p(y_1 - y_r) - k_v(y_2 - \dot{y}_r) + \ddot{y}_r \\ -k_p(z_1 - z_r) - k_v(z_2 - \dot{z}_r) + \ddot{z}_r \end{bmatrix} \end{aligned}$$

for the continuously differentiable reference $\chi_r = [x_r, y_r, z_r]^{\mathrm{T}}$. The uncertainty σ_χ does not appear in the state feedback for the same reason as the rotational dynamics. The gains (10) are the ones to achieve the optimal desired closed-loop dynamics F_χ. As in the rotational counterparts, the translational DI controller is based on the following assumptions.

Assumption 2:
1) In the domains D_χ and D_Θ, the Jacobian matrix $(\partial F_T/\partial u_t)$ is nonsingular.
2) There is a solution $u_t^* = [T_m^*, \phi_r, \theta_r]^{\mathrm{T}}$ such that $F_\chi(\chi, \Theta, u_t^*, \chi_r) = 0$ from (11).
3) $F_\chi(\chi, \Theta, u_t, \chi_r)$ is Lipschitz in its arguments on the domains D_χ, D_Θ, D_r, and D_t.
4) The uncertainties or external disturbances σ_χ and σ_Θ are continuously differentiable.

Remark 1: Our control design is differentiated from the helicopter control design [14] in the following ways. First, we define the cost functions in the multi-time-scale structure to deal with the underactuated mechanical system. By separating the helicopter dynamics into faster and slower dynamics, the mismatched disturbance issue in [14] is resolved, which results from the dynamic extension in [26, Chapter 5.4]. Second, the ENMPC in [14] utilizes the affine control inputs resulting from the approximated dynamics, which is the method often used in feedback linearization. However, our control design utilizes the DI and ENMPC to deal with the nonaffine control inputs, which results in the enlargement of the region of attraction.

B. Extended High-Gain Observer

To estimate the unmeasured system states and model uncertainties or external disturbances, we employed the EHGO as [16], [17], [27]

$$\begin{aligned}
\dot{\hat{\chi}} &= A\hat{\chi} + B\left[F_T\left(\hat{\Theta}_s, u_t\right) + \hat{\sigma}_\chi\right] + H_\chi\left(y_\chi - C\hat{\chi}\right)\\
\dot{\hat{\sigma}}_\chi &= H_{\sigma_\chi}\left(y_\chi - C\hat{\chi}\right)\\
\dot{\hat{\Theta}} &= A\hat{\Theta} + B\left[F_R\left(\hat{\Theta}_s, u_t, u_r\right) + \hat{\sigma}_\Theta\right] + H_\Theta\left(y_\Theta - C\hat{\Theta}\right)\\
\dot{\hat{\sigma}}_\Theta &= H_{\sigma_\Theta}\left(y_\Theta - C\hat{\Theta}\right)
\end{aligned} \tag{12}$$

where the estimates of χ and Θ are $\hat{\chi} = [\hat{x}_1, \hat{x}_2, \hat{y}_1, \hat{y}_2, \hat{z}_1, \hat{z}_2]^{\mathrm{T}}$ and $\hat{\Theta} = [\hat{\phi}_1, \hat{\phi}_2, \hat{\theta}_1, \hat{\theta}_2, \hat{\psi}_1, \hat{\psi}_2]^{\mathrm{T}}$, respectively. The observer gains H_χ, H_{σ_χ}, H_Θ, and H_{σ_Θ} are given as

$$\begin{aligned}
H_\chi &= \text{block diag}[H_1, H_2, H_3]\\
H_\Theta &= \text{block diag}[H_4, H_5, H_6]\\
H_i &= \left[h_{i1}/\varepsilon_4, h_{i2}/\varepsilon_4^2\right], \quad \text{for } i \in \{1, \ldots, 6\}\\
H_{\sigma_\chi} &= \text{diag}\left[h_{13}/\varepsilon_4^3, h_{23}/\varepsilon_4^3, h_{33}/\varepsilon_4^3\right]\\
H_{\sigma_\theta} &= \text{diag}\left[h_{43}/\varepsilon_4^3, h_{53}/\varepsilon_4^3, h_{63}/\varepsilon_4^3\right]
\end{aligned} \tag{13}$$

where h_{i1}, h_{i2}, and h_{i3} are chosen such that the polynomials

$$s^3 + h_{i1}s^2 + h_{i2}s + h_{i3}, \quad \text{for } i \in \{1, \ldots, 6\} \tag{14}$$

are Hurwitz.

Using the results of the EHGO, the output feedback controller is derived as

$$\begin{aligned}
\epsilon_3\dot{u}_r &= -\left(\frac{\partial F_R}{\partial u_r}\right)^{\mathrm{T}}\begin{bmatrix} k_1\left(\hat{\phi}_1 - \phi_d\right) + k_2\hat{\phi}_{2,s} + f_\phi + \hat{\sigma}_{\phi,s}\\ k_1\left(\hat{\theta}_1 - \theta_d\right) + k_2\hat{\theta}_{2,s} + f_\theta + \hat{\sigma}_{\theta,s}\\ k_1\left(\hat{\psi}_1 - \psi_r\right) + k_2\hat{\psi}_{2,s} + f_\psi + \hat{\sigma}_{\psi,s}\end{bmatrix}\\
&= -\left(\frac{\partial F_R}{\partial u_r}\right)^{\mathrm{T}} F_{\Theta_s}\left(\hat{\Theta}_s, u_r, u_t, \psi_r.\hat{\sigma}_{\Theta,s}\right)\\
\epsilon_2\dot{u}_t &= -\left(\frac{\partial F_T}{\partial u_t}\right)^{\mathrm{T}}\\
&\quad\times\begin{bmatrix} k_p(\hat{x}_1 - x_r) + k_v\left(\hat{x}_{2,s} - \dot{x}_r\right) + \left(f_x - \ddot{x}_r\right) + \hat{\sigma}_{x,s}\\ k_p(\hat{y}_1 - y_r) + k_v\left(\hat{y}_{2,s} - \dot{y}_r\right) + \left(f_y - \ddot{y}_r\right) + \hat{\sigma}_{y,s}\\ k_p(\hat{z}_1 - z_r) + k_v\left(\hat{z}_{2,s} - \dot{z}_r\right) + \left(f_z - \ddot{z}_r\right) + \hat{\sigma}_{z,s}\end{bmatrix}\\
&= -\left(\frac{\partial F_T}{\partial u_t}\right)^{\mathrm{T}} F_{\chi_s}\left(\hat{\chi}_s, \hat{\Theta}_s, u_t, \chi_r, \hat{\sigma}_{\chi,s}\right)
\end{aligned} \tag{15}$$

where $\hat{\Theta}_s = [\hat{\phi}_1, \hat{\phi}_{2,s}, \hat{\theta}_1, \hat{\theta}_{2,s}, \hat{\psi}_1, \hat{\psi}_{2,s}]^{\mathrm{T}}$, and $\hat{\chi}_s = [\hat{x}_1, \hat{x}_{2,s}, \hat{y}_1, \hat{y}_{2,s}, \hat{z}_1, \hat{z}_{2,s}]^{\mathrm{T}}$. The subscription s indicates that the values are saturated to avoid the effect of the peaking, which results in performance degradation of the EHGO

$$X_s = M_X \text{sat}\left(\frac{X}{M_X}\right) \tag{16}$$

where M_X is a saturation level of a variable X and sat$(\cdot)$ is the saturation operator. The proposed control design can be summarized in the following block diagram in Fig. 2.

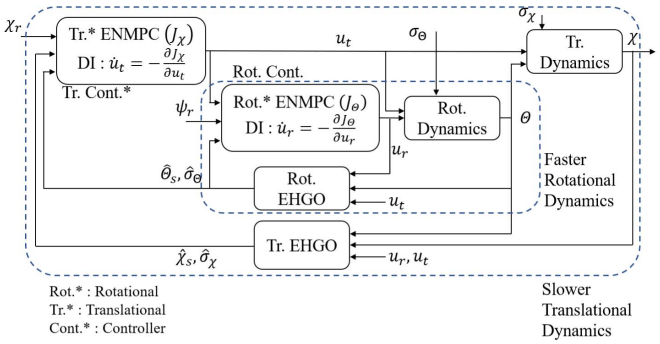

Fig. 2. Block diagram of the proposed control design.

Remark 2: We are going to describe the relationship between the time-scale structure and time horizons of the ENMPC. It is critical to choose the time horizon of the translational dynamics longer than the time horizon of the rotational dynamics, i.e., $\epsilon_t > \epsilon_r$ in (6) and (10). Since the output of the controller for the translational dynamics provides the reference of the rotational dynamics, the preview of the translational dynamics should be longer than the rotational dynamics. To satisfy this condition, the time-scale structure, i.e., the translational dynamics being slower than the rotational dynamics, is needed.

C. Stability Analysis

First, we define the error variables $e_\Theta = [e_\phi^{\mathrm{T}}, e_\theta^{\mathrm{T}}, e_\psi^{\mathrm{T}}]^{\mathrm{T}}$ of the rotational dynamics as follows:

$$\begin{aligned}
e_\phi &= \left[e_{\phi_1}, e_{\phi_2}\right]^{\mathrm{T}}, \quad e_{\phi_1} = \phi_1 - \phi_r, \ e_{\phi_2} = \epsilon_r\phi_2\\
e_\theta &= \left[e_{\theta_1}, e_{\theta_2}\right]^{\mathrm{T}}, \quad e_{\theta_1} = \theta_1 - \theta_r, \ e_{\theta_2} = \epsilon_r\theta_2\\
e_\psi &= \left[e_{\psi_1}, e_{\psi_2}\right]^{\mathrm{T}}, \quad e_{\psi_1} = \psi_1 - \psi_r, \ e_{\psi_2} = \epsilon_r\psi_2
\end{aligned} \tag{17}$$

where ϕ_r and θ_r are the elements of u_t^*. The rotational error dynamics is

$$\epsilon_r\dot{e}_\Theta = (A - BL_\Theta)e_\Theta - \epsilon_r B_2\dot{\Theta}_r + \epsilon_r^2 BE_\Theta + k_{pr}B(\Theta_d - \Theta_r) \tag{18}$$

where $\Theta_r = [\phi_r, \theta_r, \psi_r]^{\mathrm{T}}$, $\Theta_d = [\phi_d, \theta_d, \psi_r]^{\mathrm{T}}$, $B_2 = \text{block diag } [B_b, B_b, B_b]$ with $B_b = [1, 0]^{\mathrm{T}}$, and E_Θ and L_Θ are

$$\begin{aligned}
E_\Theta &= F_R(\Theta, u_t, u_r) - F_R\left(\Theta, u_t, u_r^*\right)\\
L_\Theta &= \text{block diag } [L_r, L_r, L_r], \quad L_r = \left[k_{pr}, k_{vr}\right]
\end{aligned} \tag{19}$$

with $k_{pr} = 10/3$ and $k_{vr} = 5/2$ from (6).

The error variables for the translational dynamics $e_\chi = [e_x^{\mathrm{T}}, e_y^{\mathrm{T}}, e_z^{\mathrm{T}}]^{\mathrm{T}}$ are defined as

$$e_x = \left[e_{x_1}, e_{x_2}\right]^{\mathrm{T}}, \quad e_{x_1} = x_1 - x_r, \ e_{x_2} = \epsilon_t(x_2 - \dot{x}_r)$$

$$e_y = \left[e_{y_1}, e_{y_2}\right]^{\mathrm{T}}, \quad e_{y_1} = y_1 - y_r, \ e_{y_2} = \epsilon_t(y_2 - \dot{y}_r)$$
$$e_z = \left[e_{z_1}, e_{z_2}\right]^{\mathrm{T}}, \quad e_{z_1} = z_1 - z_r, \ e_{z_2} = \epsilon_t(z_2 - \dot{z}_r). \tag{20}$$

The translational error dynamics is given as follows:

$$\epsilon_t \dot{e}_\chi = \left(A - BL_\chi\right)e_\chi + \epsilon_t^2 B E_\chi \tag{21}$$

where L_χ = block diag $[L_t, L_t, L_t]$, $L_t = [k_{pt}, k_{vt}]$, and $E_\chi = F_T(\Theta, u_t) - F_T(\Theta, u_t^*)$, with $k_{pt} = 10/3$ and $k_{vt} = 5/2$ from (10). The error dynamics for the rotational and the translational DIs [17] are

$$\epsilon_3 \dot{s}_r = -\left(\frac{\partial F_R}{\partial u_r}\right)^{\mathrm{T}}\left[F_\Theta(\Theta, u_t, u_r, \psi_r) + \bar{E}_\Theta\right] - \epsilon_3 \dot{u}_r^*$$
$$\epsilon_2 \dot{s}_t = -\left(\frac{\partial F_T}{\partial u_t}\right)^{\mathrm{T}}\left[F_\chi(\Theta, \chi, u_t, \chi_r) + \bar{E}_\chi\right] - \epsilon_2 \dot{u}_t^* \tag{22}$$

where $s_r = u_r - u_r^*$ and $s_t = u_t - u_t^*$ are the error variables for the translational controller and the rotational controller, respectively, with $\bar{E}_\Theta = F_{\Theta_s} - F_\Theta$ and $\bar{E}_\chi = F_{\chi_s} - F_\chi$.

The fast error variables $\eta = [\eta_\chi^{\mathrm{T}}, \eta_\Theta^{\mathrm{T}}]^{\mathrm{T}}$ for the EHGO are given by $\eta_\chi = [\eta_x^{\mathrm{T}}, \eta_y^{\mathrm{T}}, \eta_z^{\mathrm{T}}]^{\mathrm{T}}$ and $\eta_\Theta = [\eta_\phi^{\mathrm{T}}, \eta_\theta^{\mathrm{T}}, \eta_\psi^{\mathrm{T}}]^{\mathrm{T}}$, where

$$\eta_\varphi = \left[\eta_{\varphi_1}, \eta_{\varphi_2}, \eta_{\varphi_3}\right]^{\mathrm{T}}$$
$$\eta_{\varphi_1} = \frac{\varphi_1 - \hat{\varphi}_1}{\epsilon_4^2}, \quad \eta_{\varphi_2} = \frac{\varphi_2 - \hat{\varphi}_2}{\epsilon_4}, \ \eta_{\varphi_3} = \sigma_\varphi - \hat{\sigma}_\varphi \tag{23}$$

for $\varphi \in \{x, y, z, \phi, \theta, \psi\}$. The error dynamics for the EHGO are

$$\epsilon_4 \dot{\eta} = \bar{A}\eta + \epsilon_4\left[\bar{B}_1\Delta_1 + \bar{B}_2\Delta_2\right] \tag{24}$$

where

$$\bar{A} = \text{block diag}\left[\bar{A}_1, \ldots, \bar{A}_1\right] \in \mathbb{R}^{18\times 18}$$
$$\bar{B}_1 = \text{block diag}\left[\bar{B}_a, \ldots, \bar{B}_a\right] \in \mathbb{R}^{18\times 6}$$
$$\bar{B}_2 = \text{block diag}\left[\bar{B}_b, \ldots, \bar{B}_b\right] \in \mathbb{R}^{18\times 6}$$
$$\bar{A}_1 = \begin{bmatrix} 0 & 1 & 0 \\ 0 & 0 & 0 \\ 0 & 0 & 0 \end{bmatrix}, \quad \bar{B}_a = \begin{bmatrix} 0 \\ 1 \\ 0 \end{bmatrix}, \ \bar{B}_b = \begin{bmatrix} 0 \\ 0 \\ 1 \end{bmatrix}$$
$$\Delta_1 = \frac{1}{\epsilon_4}\begin{bmatrix} F_T(\Theta, u_t) - F_T\left(\hat{\Theta}_s, u_t\right) \\ F_R(\Theta, u_t, u_r) - F_R\left(\hat{\Theta}_s, u_t, u_r\right) \end{bmatrix}$$
$$\Delta_2 = \left[\dot{\sigma}_x, \dot{\sigma}_y, \dot{\sigma}_z, \dot{\sigma}_\phi, \dot{\sigma}_\theta, \dot{\sigma}_\psi\right]^{\mathrm{T}}. \tag{25}$$

Now, we will describe the theorem. The stability analysis for the closed-loop system is motivated by the works regarding the multi-time-scale framework [16], [17], [27], [28].

Theorem 1: Assumptions 1 and 2 are satisfied. Let X_1 be any compact set of $(\chi, \Theta) \in D_\chi \times D_\Theta$, X_2 be any compact subset of $\mathbb{R}^6$, and X_3 be any compact subset of $\mathbb{R}^{12}$. Then, the closed-loop system (18), (21), (22), and (24) is asymptotically stable in its domains D_χ, D_Θ, D_r, and D_t with the time scales given by

$$\epsilon_r \ll \epsilon^*, \quad \epsilon_2 \ll \epsilon^*, \quad \epsilon_3 \ll \epsilon^*, \quad \epsilon_4 \ll \epsilon^*$$
$$(\epsilon_r/\epsilon_t) \ll \epsilon^*, \quad (\epsilon_3/\epsilon_2) \ll \epsilon^*, \ (\epsilon_4/\epsilon_3) \ll \epsilon^* \tag{26}$$

for $0 < \epsilon^* \ll 1$ and for the initial states $(\chi(0), \Theta(0)) \in X_1$, $(u_t(0), u_r(0)) \in X_2$, and $(\hat{\chi}(0), \hat{\Theta}(0)) \in X_3$.

Proof: Based on the error variables, we take the approximated rotational cost functions J_Θ and J_χ and consider it as a part of the Lyapunov function. Note that the approximated cost functions are not a time integral of a function, but a constant, since we approximated the cost function using the Taylor-series expansion and solved it explicitly.

$$V_\Theta = \left[e_\Theta^{\mathrm{T}}\ (F_R + \sigma_\Theta)^{\mathrm{T}}\right]\begin{bmatrix} \Gamma_{R_1} & \Gamma_{R_2} \\ \Gamma_{R_2}^{\mathrm{T}} & \Gamma_{R_3} \end{bmatrix}\begin{bmatrix} e_\Theta \\ F_R + \sigma_\Theta \end{bmatrix}$$
$$= J_\Theta(e_\Theta, F_R, \sigma_\Theta) = J_\Theta(e_\Theta, \Theta, u_t, u_r, \sigma_\Theta) \tag{27}$$

where Γ_{R_i} = block diag $[K_{R_i}, K_{R_i}, K_{R_i}]$, for $i \in \{1, 2, 3\}$, with

$$K_{R_1} = \begin{bmatrix} \epsilon_r & \epsilon_r/2 \\ \epsilon_r/2 & \epsilon_r/3 \end{bmatrix}, \quad K_{R_2} = \begin{bmatrix} \epsilon_r^3/6 \\ \epsilon_r^3/8 \end{bmatrix}, \ K_{R_3} = \epsilon_r^5/20.$$

Likewise, the approximated cost function for the translational dynamics J_χ is modified as

$$V_\chi = \left[e_\chi^{\mathrm{T}}\ \left(F_T + \sigma_\chi\right)^{\mathrm{T}}\right]\begin{bmatrix} \Gamma_{T_1} & \Gamma_{T_2} \\ \Gamma_{T_2}^{\mathrm{T}} & \Gamma_{T_3} \end{bmatrix}\begin{bmatrix} e_\chi \\ F_T + \sigma_\chi \end{bmatrix}$$
$$= J_\chi\left(e_\chi, F_T, \sigma_\chi\right) = J_\chi\left(e_\chi, \Theta, u_t, \sigma_\chi\right) \tag{28}$$

where Γ_{T_i} = block diag $[K_{T_i}, K_{T_i}, K_{T_i}]$, for $i \in \{1, 2, 3\}$, with

$$K_{T_1} = \begin{bmatrix} \epsilon_t & \epsilon_t/2 \\ \epsilon_t/2 & \epsilon_t/3 \end{bmatrix}, \quad K_{T_2} = \begin{bmatrix} \epsilon_t^3/6 \\ \epsilon_t^3/8 \end{bmatrix}, \ K_{T_3} = \epsilon_t^5/20.$$

Considering relations between the trajectories χ and e_χ, and Θ and e_Θ, it is worth to note that

$$\left(e_\chi, e_\Theta\right) \in \left\{V_\chi \le a_1\right\} \times \left\{V_\Theta \le a_2\right\} \implies (\chi, \Theta) \in X_1 \tag{29}$$

i.e., e_χ and e_Θ are on its own ellipsoids. Note that the radii of the ellipsoids are chosen by the selection of the time horizon as (27) and (28). The derivative of the rotational Lyapunov function V_Θ is derived as follows:

$$\dot{V}_\Theta = \left(\frac{\partial J_\Theta}{\partial e_\Theta}\right)^{\mathrm{T}}\dot{e}_\Theta + \left(\frac{\partial J_\Theta}{\partial \Theta}\right)^{\mathrm{T}}\dot{\Theta} + \left(\frac{\partial J_\Theta}{\partial u_r}\right)^{\mathrm{T}}\dot{u}_r + \left(\frac{\partial J_\Theta}{\partial u_t}\right)^{\mathrm{T}}\dot{u}_t + \left(\frac{\partial J_\Theta}{\partial \sigma_\Theta}\right)^{\mathrm{T}}\dot{\sigma}_\Theta$$
$$= \left(\frac{\partial J_\Theta}{\partial e_\Theta}\right)^{\mathrm{T}}\left(\frac{1}{\epsilon_r}A_\Theta e_\Theta - B_2\dot{\Theta}_r + \epsilon_r B E_\Theta + \frac{k_{pr}}{\epsilon_r}B(\Theta_d - \Theta_r)\right)$$
$$+ \left(\frac{\partial J_\Theta}{\partial \Theta}\right)^{\mathrm{T}}(A\Theta + BF_R) - \frac{1}{\epsilon_2}\left(\frac{\partial J_\Theta}{\partial u_t}\right)^{\mathrm{T}}\left(\frac{\partial F_T}{\partial u_t}\right)^{\mathrm{T}}F_{\chi_s}$$
$$- \frac{1}{\epsilon_3}F_\Theta^{\mathrm{T}}\left(\frac{\partial F_R}{\partial u_r}\right)\left(\frac{\partial F_R}{\partial u_r}\right)^{\mathrm{T}}F_\Theta - \frac{1}{\epsilon_3}F_\Theta^{\mathrm{T}}\left(\frac{\partial F_R}{\partial u_r}\right)\left(\frac{\partial F_R}{\partial u_r}\right)^{\mathrm{T}}\bar{E}_\Theta$$
$$+ \left(\frac{\partial J_\Theta}{\partial \sigma_\Theta}\right)^{\mathrm{T}}\dot{\sigma}_\Theta \tag{30}$$

where $A_\Theta = A - BL_\Theta$ and $\bar{E}_\Theta = F_{\Theta_s} - F_\Theta$.

Based on the time scale (26),

$$\dot{V}_\Theta \le \left(\frac{1}{\epsilon_r}k_{r_1}\|e_\Theta\| + k_{r_2}\|\dot{\Theta}_r\| + k_{r_3}\epsilon_r\|s_r\| + k_{r_4}\right)k_{r_5}$$
$$+ k_{r_6} + \frac{1}{\epsilon_2}k_{r_7}\|F_{\chi_s}\| - \frac{1}{\epsilon_3}\left\|\frac{\partial J_\Theta}{\partial u_r}\right\|^2 + \frac{1}{\epsilon_3}k_{r_8}\|\eta\|\|F_\Theta\|$$
$$+ k_{r_9}\|\dot{\sigma}_\Theta\| < 0 \tag{31}$$

where k_{r_i} for $i \in \{1, \ldots, 9\}$ are positive constants regarding the boundaries. Similarly, the derivative of the translational Lyapunov function V_χ is

$$\dot{V}_\chi = \left(\frac{\partial J_\chi}{\partial e_\chi}\right)^{\mathrm{T}}\dot{e}_\chi + \left(\frac{\partial J_\chi}{\partial \Theta}\right)^{\mathrm{T}}\dot{\Theta} + \left(\frac{\partial J_\chi}{\partial u_t}\right)^{\mathrm{T}}\dot{u}_t + \left(\frac{\partial J_\chi}{\partial \sigma_\chi}\right)^{\mathrm{T}}\dot{\sigma}_\chi$$

$$= \left(\frac{\partial J_\chi}{\partial e_\chi}\right)^{\mathrm{T}}\left(\frac{1}{\epsilon_t}A_\chi e_\chi + \epsilon_t B E_\chi\right) + \left(\frac{\partial J_\chi}{\partial \Theta}\right)^{\mathrm{T}}(A\Theta + BF_R) - \frac{1}{\epsilon_2}F_\chi^{\mathrm{T}}\left(\frac{\partial F_T}{\partial u_t}\right)\left(\frac{\partial F_T}{\partial u_t}\right)^{\mathrm{T}}F_\chi - \frac{1}{\epsilon_2}F_\chi^{\mathrm{T}}\left(\frac{\partial F_T}{\partial u_t}\right)\left(\frac{\partial F_T}{\partial u_t}\right)^{\mathrm{T}}\bar{E}_\chi + \left(\frac{\partial J_\chi}{\partial \sigma_\chi}\right)^{\mathrm{T}}\dot{\sigma}_\chi \quad (32)$$

where $A_\chi = A - BL_\chi$ and $\bar{E}_\chi = F_{\chi_s} - F_\chi$. Taking $\epsilon_t \sim 1$ for the sake of convenience, its inequality is given as follows:

$$\dot{V}_\chi \leq \left(k_{t_1}\|e_\chi\| + k_{t_2}\|s_t\|\right)k_{t_3} + k_{t_4} - \frac{1}{\epsilon_2}\left\|\frac{\partial J_\chi}{\partial u_t}\right\|^2 + \frac{1}{\epsilon_2}k_{t_5}\|\eta\|\|F_\chi\| + k_{t_6}\|\dot{\sigma}_\chi\| < 0 \quad (33)$$

where k_{t_j} for $j \in \{1, \ldots, 6\}$ are positive constants regarding the boundaries. The saturation (16) has been adopted to avoid the peaking phenomenon [27]. As mentioned in [29], the peaking period shrinks to zero for sufficiently small ϵ_4 and does not affect much to the closed-loop stability. Therefore, the saturation period can be omitted in the stability analysis. We take the Lyapunov functions for the faster dynamics, such as the DIs and the EHGO, from [17]. The Lyapunov functions for the DI are given as $V_r = F_\Theta^{\mathrm{T}}F_\Theta$ and $V_t = F_\chi^{\mathrm{T}}F_\chi$ for the rotational and translational DI, respectively. Finally, the Lyapunov function for the EHGO is $V_\eta = \eta^{\mathrm{T}}P_\eta\eta$, where $\bar{A}P_\eta + P_\eta\bar{A}^{\mathrm{T}} = -I$. The rest of the proof is similar to that of Chapter 3.3.4 of [17] and can be analyzed easily using the method in Section 9.3 of [30], thus omitted in this brief due to the page limit. □

IV. Experimental Tests

This section is organized as follows. First, the proposed control design is discretized for implementation. Second, the benchmark results using the numerical simulation are presented. Third, the hardware setup for the experimental test is briefly explained. Finally, outdoor experimental test results are presented.

A. Controller Discretization

1) Extended High-Gain Observers: To attenuate the noise amplification, the second-order EHGO is utilized as follows:

$$\begin{aligned}\hat{\mathcal{X}}(k+1) &= \hat{\mathcal{X}}(k) + T\left[F_T\left(\hat{\Theta}_e, u_t\right) + \hat{\sigma}_\chi + H_{\mathcal{X}}\left(\mathcal{X} - \hat{\mathcal{X}}\right)\right]\\ \hat{\sigma}_\chi(k+1) &= \hat{\sigma}_\chi(k) + T\left[H_{\sigma_\chi}\left(\mathcal{X} - \hat{\mathcal{X}}\right)\right]\\ \hat{\vartheta}(k+1) &= \hat{\vartheta}(k) + T\left[F_R\left(\hat{\Theta}_e, u_t, u_r\right) + \hat{\sigma}_\Theta + H_\vartheta\left(\vartheta - \hat{\vartheta}\right)\right]\\ \hat{\sigma}_\Theta(k+1) &= \hat{\sigma}_\Theta(k) + T\left[H_{\sigma_\Theta}\left(\vartheta - \hat{\vartheta}\right)\right]\end{aligned} \quad (34)$$

where $\mathcal{X} = [x_2, y_2, z_2]^{\mathrm{T}}$, $\vartheta = [\phi_2, \theta_2, \psi_2]^{\mathrm{T}}$, $\hat{\Theta}_e = [\phi_1, \phi_{2,s}, \theta_1, \theta_{2,s}, \psi_1, \psi_{2,s}]^{\mathrm{T}}$,

$$H_{\mathcal{X}} = \frac{1}{\epsilon_4}\mathrm{diag}[h_{11}, h_{21}, h_{31}], \quad H_\vartheta = \frac{1}{\epsilon_4}\mathrm{diag}[h_{41}, h_{51}, h_{61}]$$
$$H_{\sigma_\chi} = \frac{1}{\epsilon_4^2}\mathrm{diag}[h_{12}, h_{22}, h_{32}], \quad H_{\sigma_\Theta} = \frac{1}{\epsilon_4^2}\mathrm{diag}[h_{42}, h_{52}, h_{62}] \quad (35)$$

and T is a sampling period. The observer gains are selected such that the polynomials $s^2 + h_{i1}s + h_{i2}$ for $i = 1, \ldots, 6$ are Hurwitz.

TABLE I
RMSe Value Measured in the Simulation Experiment

	ENMPC	DOB-CSMC	DI-ENMPC (proposed)
RMSe value	0.4982	0.4338	0.3494

2) Rotational and Translational Controllers: Using estimated states and uncertainties in (34), the DI-ENMPC controllers are discretized using the forward difference method. In the discretization process, the saturation and the low-pass filters are added to the control inputs to make the control signals less noisy as follows:

$$\begin{aligned}C_t(k+1) &= C_t(k) + \alpha_t \odot \left[u_{t,s}(k) - C_t(k)\right]\\ C_r(k+1) &= C_r(k) + \alpha_r \odot \left[u_{r,s}(k) - C_r(k)\right]\\ u_{t,s} &= M_t \odot \mathrm{sat}(u_t \oslash M_t), \quad u_{r,s} = M_r \odot \mathrm{sat}(u_r \oslash M_r)\end{aligned} \quad (36)$$

where $\odot$ is elementwise multiplication, $\oslash$ is elementwise division, $\mathrm{sat}(\cdot)$ is an saturation operator, $M_t = [M_{t,1}, M_{t,2}, M_{t,3}]^{\mathrm{T}}$ and $M_r = [M_{r,1}, M_{r,2}, M_{r,3}]^{\mathrm{T}}$ are saturation levels for each control input, and C_t and C_r are control signals of the translational and the rotational dynamics, respectively. The saturation levels are selected considering the actuator limits.

B. Benchmark Simulation Results

To show the outperformance of our control design (DI-ENMPC), we applied the control design proposed in [14], an ENMPC, and [10], a DOB-CSMC. The controllers are formulated in discrete time with a sampling frequency of 250 Hz. We employed a simple disturbance observer proposed in [31] for the ENMPC and the DOB-CSMC. We have improved the ENMPC using the methods suggested in [31] to deal with the mismatched disturbances. We used the system parameters obtained in the hardware experiment, and the gains are selected using the methods in each paper—see the supplementary material for the details. We utilized the sum of the root-mean-squared error (RMSe) as a performance parameter, i.e., $\mathrm{RMSe} = \mathrm{rms}(e_x) + \mathrm{rms}(e_y) + \mathrm{rms}(e_z) + \mathrm{rms}(e_\psi)$, and the results are presented in the Table I. As a result, the DI-ENMPC has improved the RMSe value by 29.87% compared to ENMPC and 19.46% compared to DOB-CSMC. The trajectories and control inputs are plotted in the Supplementary Material. In Fig. S5, the trajectories x_1, y_1, z_1, and ψ_1 are shown. The trajectories of the DI-ENMPC showed the best and the fastest convergence compared to ENMPC and DOB-CSMC. In Fig. S7, the trajectories ϕ_1 and θ_1 are plotted. Compared to DOB-CSMC, the DI-ENMPC showed more aggressive behavior. In the Supplementary Material, we presented the results for the rotational dynamics. When the same references are given, we have shown that the DI-ENMPC performs better than other benchmark controls. This can be interpreted as the effects of the enlarged region of attraction.

C. Hardware Setup

We use an embedded board, *Pixhawk* 4 [32], and a small-scale helicopter platform, *Walkera V450D03*. *Walkera*

V450D03 is a 450-class helicopter model with a swashplate composed of three RC servo motors and the brushless dc (BLDC) motor. The BLDC motor rotates both the main rotor and tail rotor. Additional RC servo motor at the tail rotor (rudder servo motor) controls its angle of attack. Pixhawk provides the vehicle's estimated attitude in Euler angles and local positions in x, y, z coordinates. A 6-DOF (degrees of freedom) gyroscope and a 3-DOF magnetometer are used to estimate the helicopter's attitude; a GPS and a barometric pressure sensor are employed to estimate local positions with the 250 Hz of the sampling frequency. The overall hardware setup can be found in the Supplementary Material. The control design is realized through the embedded coder toolbox for pixhawk autopilot in *MATLAB/Simulink* environment [33]. The translational and rotational controllers and the EHGO are formulated in a single loop with 250 Hz of the sampling frequency. In addition, the actuator modeling and parameter estimation are conducted as presented in Section S2 of the Supplementary Material.

D. Experimental Results

The control and observer gains used throughout the experiments are selected as follows:

$$\begin{aligned} h_{i1} &= 3, \quad [h_{12}, h_{22}, h_{32}] = [0.2, 0.1, 1] \\ h_{j1} &= 4, \quad [h_{42}, h_{52}, h_{62}] = [0.2, 0.25, 0.25] \end{aligned} \tag{37}$$

for $i \in \{1, 2, 3\}$ and $j \in \{4, 5, 6\}$. The time scales are selected as

$$\begin{aligned} \epsilon_t &= 1.5, \quad \epsilon_r = 0.275 \\ \epsilon_{2_{x,y}} &= 0.25, \quad \epsilon_{2_z} = 0.1, \ \epsilon_3 = 0.1, \ \epsilon_4 = 0.08 \end{aligned} \tag{38}$$

which satisfies the condition of (26). The gains for the low-pass filters are $\alpha_t = [0.15, 0.15, 0.95]^{\mathrm{T}}$ and $\alpha_r = [0.02, 0.02, 0.02]^{\mathrm{T}}$. The time-scales and low-pass filter gains are chosen to adapt the control input dynamics in the z-direction (T_m). Finally, the saturation limits for the control inputs are selected as $M_t = [18, 0.5, 0.5]^{\mathrm{T}}$ and $M_r = [5, \pi/6, \pi/6]^{\mathrm{T}}$.

Remark 3: The practical procedure for selecting the gains ϵ_t, ϵ_r, ϵ_2, ϵ_3, and ϵ_4 is provided as follows.

1) First, select M_r to consider the hardware capacity. Then, tune ϵ_r and ϵ_3, until the state feedback controller stabilizes the rotational dynamics and satisfies the performance.
2) Second, select M_t to consider the hardware capacity. Then, select ϵ_t such that $(\epsilon_t/\epsilon_r) \ll \epsilon^*$ and ϵ_2 such that $(\epsilon_2/\epsilon_3) \ll \epsilon^*$, where $0 < \epsilon^* \ll 1$. Tune the gains until the helicopter performance is satisfied for the position holding and trajectory tracking.
3) Third, record the amplitudes of the states χ and Θ under the state feedback to determine the saturation levels of the EHGO, so that the saturation is not activated during the flight.
4) Finally, select ϵ_4 such that $(\epsilon_3/\epsilon_4) \ll \epsilon^*$. Validate the estimated performance.

Two different experimental tests (position holding and tracking the reference trajectories) were conducted as follows.

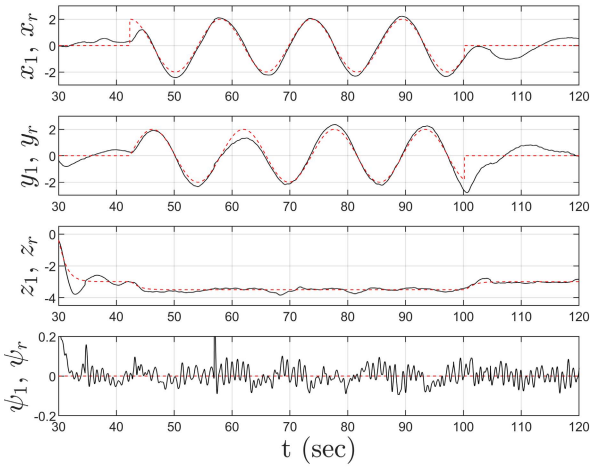

Fig. 3. Solid lines represent trajectories x_1, y_1, z_1, and ψ_1. Dashed lines represent the references, while solid lines represent the trajectories (units: m for x, y, and z and rad for ψ_1).

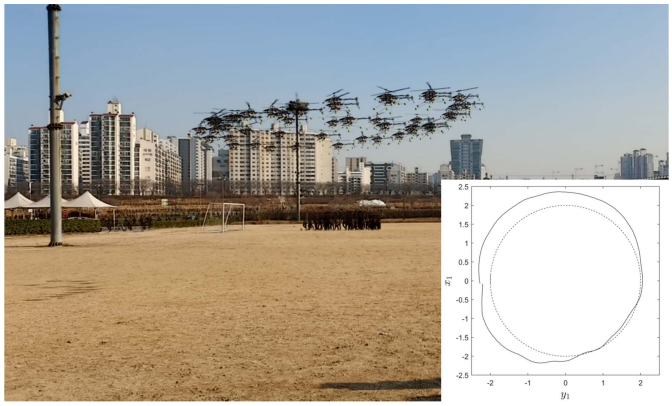

Fig. 4. Circular trajectory is shown in frame by frame images of the experiment. The trajectory (solid-line) and its reference (dotted-line) of one cycle during the experiment.

First, the position holding experimental test is to locate the helicopter at the position as $x_r = 0$ (m), $y_r = 0$ (m), $z_r = -3.5$ (m), and $\psi_r = 0$ (rad). Second, for experimental tests to track a reference, the reference is begin by $x_r = 2\cos 0.4t$ (m), $y_r = 2\sin 0.4t$ (m), $z_r = -4.0$ (m), and $\psi_r = 0$ (rad). The derivatives of the references are obtained by numerical differentiation of x_r and y_r. The z_r reference are filtered with a second-order low-pass filter. Fig. 3 shows that the experiments begin with position holding starting at 30 s and ends at 42 s, tracking reference experimental test starts at 42 s and ends at 100 s, and position holding for the final stage starts at 100 s.

The time lapse to track the circular trajectory during the experiment is plotted in Fig. 4. In Fig. S14, the system states ϕ_1, θ_1, and ψ_1 and references ϕ_d, θ_d, and ψ_r are shown. The reference signals ϕ_d and θ_d are from the translational DI. ϕ_1, θ_1, and ψ_1 track the reference trajectories. The estimates $\hat{\mathcal{X}}$ and $\hat{\vartheta}$ from the EHGO and measurements $\mathcal{X}$ and ϑ from sensors are plotted in Figs. S13 and S15, respectively. The EHGO estimates the signals well, and amplified plots are shown on the right-hand side at each subplot. The estimated uncertainties for the translational and the rotational dynamics

are shown in Figs. S16 and S17, respectively. The actual helicopter control inputs T_m, T_t, a_{1s}, and b_{1s} in the experiment are shown in Fig. S18.

In conclusion, in contrast to the vision localization-based indoor experiments [14], our successful outdoor experiment clearly shows that our control design can be implemented with the off-the-shelf Pixhawk device.

V. Conclusion

In this brief, the novel control design for a helicopter under external disturbances and model uncertainties using nonaffine control inputs was proposed. Based on the time-scale separation, the ENMPC was utilized for optimal trajectory tracking and to provide the framework for the DIs. The DI dealt with nonaffine control inputs and the EHGO estimated uncertainties. The stability of the closed-loop system in the continuous time was analyzed. The outperformance of our control design was demonstrated by the discrete-time simulation by comparing the benchmark controllers. The proposed control design was validated through the outdoor experimental tests in the presence of external disturbances and model uncertainties. The proposed control design was implemented to a small-scale helicopter with Pixhawk 4. In the experimental tests, the effectiveness of the proposed control design was shown.

Appendix
Video of the Experiment in the Outdoor

The video of the experiment done in the outdoor can be found in the following link: https://youtu.be/aLQ-Ar9PMv4.

References

[1] K. Sprague, V. Gavrilets, D. Dugail, B. Mettler, E. Feron, and I. Martinos, "Design and applications of an avionics system for a miniature acrobatic helicopter," in *Proc. 20th DASC. 20th Digit. Avionics Syst. Conf.*, vol. 1, Oct. 2001, p. 3C5–1.

[2] C. Zhang and J. M. Kovacs, "The application of small unmanned aerial systems for precision agriculture: A review," *Precis. Agricult.*, vol. 13, no. 6, pp. 693–712, Dec. 2012.

[3] D. Shim, H. Chung, H. J. Kim, and S. Sastry, "Autonomous exploration in unknown urban environments for unmanned aerial vehicles," in *Proc. AIAA Guid., Navigat., Control Conf. Exhib.*, Aug. 2005, p. 6478.

[4] F. Leonard, A. Martini, and G. Abba, "Robust nonlinear controls of model-scale helicopters under lateral and vertical wind gusts," *IEEE Trans. Control Syst. Technol.*, vol. 20, no. 1, pp. 154–163, Jan. 2012.

[5] I. A. Raptis, K. P. Valavanis, and G. J. Vachtsevanos, "Linear tracking control for small-scale unmanned helicopters," *IEEE Trans. Control Syst. Technol.*, vol. 20, no. 4, pp. 995–1010, Jul. 2012.

[6] Y. Zou and Z. Zheng, "A robust adaptive RBFNN augmenting backstepping control approach for a model-scaled helicopter," *IEEE Trans. Control Syst. Technol.*, vol. 23, no. 6, pp. 2344–2352, Nov. 2015.

[7] S. Lee, C. Ha, and B. S. Kim, "Adaptive nonlinear control system design for helicopter robust command augmentation," *Aerosp. Sci. Technol.*, vol. 9, no. 3, pp. 241–251, Apr. 2005.

[8] A. Isidori, L. Marconi, and A. Serrani, "Robust nonlinear motion control of a helicopter," in *Robust Autonomous Guidance*. Cham, Switzerland: Springer, 2003, pp. 149–192.

[9] C. Ha, Z. Zuo, F. B. Choi, and D. Lee, "Passivity-based adaptive backstepping control of quadrotor-type UAVs," *Robot. Auto. Syst.*, vol. 62, no. 9, pp. 1305–1315, Sep. 2014.

[10] X. Fang and Y. Shang, "Trajectory tracking control for small-scale unmanned helicopters with mismatched disturbances based on a continuous sliding mode approach," *Int. J. Aerosp. Eng.*, vol. 2019, pp. 1–15, Apr. 2019.

[11] M. Mehndiratta and E. Kayacan, "Online learning-based receding horizon control of tilt-rotor tricopter: A cascade implementation," in *Proc. Annu. Amer. Control Conf. (ACC)*, Jun. 2018, pp. 6378–6383.

[12] M. Chen, S. S. Ge, and B. Ren, "Robust attitude control of helicopters with actuator dynamics using neural networks," *IET Control Theory Appl.*, vol. 4, no. 12, pp. 2837–2854, Dec. 2010.

[13] G. Shi *et al.*, "Neural Lander: Stable drone landing control using learned dynamics," in *Proc. Int. Conf. Robot. Autom. (ICRA)*, May 2019, pp. 9784–9790.

[14] C. Liu, W.-H. Chen, and J. Andrews, "Tracking control of small-scale helicopters using explicit nonlinear MPC augmented with disturbance observers," *Control Eng. Pract.*, vol. 20, no. 3, pp. 258–268, Mar. 2012.

[15] T. J. Koo and S. Sastry, "Output tracking control design of a helicopter model based on approximate linearization," in *Proc. 37th IEEE Conf. Decis. Control*, vol. 4, Dec. 1998, pp. 3635–3640.

[16] J. Lee, R. Mukherjee, and H. K. Khalil, "Control design for a helicopter using dynamic inversion and extended high gain observers," in *Proc. Legged Locomotion, Mech. Syst., Mechatronics, Mechatronics Aquatic Environ., MEMS Control, Model Predictive Control, Modeling Model-Based Control Adv. IC Engines*, Oct. 2012, pp. 653–660.

[17] J. Lee, "Output feedback control in the presence of uncertainties: Using extended high-gain observers with dynamic inversion," Ph.D. dissertation, Michigan State Univ., East Lancing, MI, USA, 2014.

[18] C. J. Boss, J. Lee, C. C. De Aguiar, and J. Choi, "Implementation of state and disturbance estimation for quadrotor control using extended high-gain observers," in *Proc. Dyn. Syst. Control Conf.* New York, NY, USA: American Society of Mechanical Engineers, 2016, Art. no. V002T17A006.

[19] C. J. Boss, J. Lee, and J. Choi, "Uncertainty and disturbance estimation for quadrotor control using extended high-gain observers: Experimental implementation," in *Proc. Dyn. Syst. Control Conf.* New York, NY, USA: American Society of Mechanical Engineers, 2017, Art. no. V002T01A003.

[20] J. Seo and J. Choi, "Output feedback control synthesis for a helicopter using explicit nonlinear model predictive control, dynamic inversion and extended high gain observers," in *Proc. Dyn. Syst. Control Conf.* New York, NY, USA: American Society of Mechanical Engineers Digital Collection, 2019.

[21] L. Marconi and R. Naldi, "Aggressive control of helicopters in presence of parametric and dynamical uncertainties," *Mechatronics*, vol. 18, no. 7, pp. 381–389, Sep. 2008.

[22] W.-H. Chen, D. J. Ballance, and P. J. Gawthrop, "Optimal control of nonlinear systems: A predictive control approach," *Automatica*, vol. 39, no. 4, pp. 633–641, Apr. 2003.

[23] N. Hovakimyan, E. Lavretsky, and A. J. Sasane, "Dynamic inversion for nonaffine-in-control systems via time-scale separation: Part I," in *Proc. Amer. Control Conf.*, 2005, pp. 3542–3547.

[24] J. Teo and J. P. How, "Equivalence between approximate dynamic inversion and proportional-integral control," in *Proc. 47th IEEE Conf. Decis. Control*, 2008, pp. 2179–2183.

[25] E. Lavretsky and N. Hovakimyan, "Adaptive dynamic inversion for nonaffine-in-control systems via time-scale separation: Part II," in *Proc. Amer. Control Conf.*, 2005, pp. 3548–3553.

[26] A. Isidori, *Nonlinear Control Systems*. Cham, Switzerland: Springer, 2013.

[27] J. Lee, R. Mukherjee, and H. K. Khalil, "Output feedback performance recovery in the presence of uncertainties," *Syst. Control Lett.*, vol. 90, pp. 31–37, Apr. 2016.

[28] L. B. Freidovich and H. K. Khalil, "Performance recovery of feedback-linearization-based designs," *IEEE Trans. Autom. Control*, vol. 53, no. 10, pp. 2324–2334, Nov. 2008.

[29] H. K. Khalil, "High-gain observers in nonlinear feedback control," in *Proc. IEEE Int. Conf. Control Autom.*, Dec. 2009, pp. 47–57.

[30] H. K. Khalil and J. W. Grizzle, *Nonlinear System*, vol. 3. Upper Saddle River, NJ, USA: Prentice-Hall, 2002.

[31] X. Fang, A. Wu, Y. Shang, and N. Dong, "Robust control of small-scale unmanned helicopter with matched and mismatched disturbances," *J. Franklin Inst.*, vol. 353, no. 18, pp. 4803–4820, Dec. 2016.

[32] (2020). [Online]. Available: https://docs.px4.io/v1.9.0/en/flight_controller/pixhawk4.html

[33] *Px4 Autopilots Support From Embedded Coder*, The MathWorks, Natick, MA, USA, 2019. [Online]. Available: https://mathworks.com/hardware-support/px4-autopilots.html